This is a preprint, the final version is subject to change, of the American Mineralogist (MSA)
Cite as Authors (Year) Title. American Mineralogist, in press.
DOI: https://doi.org/10.2138/am-2020-7339

Revision 1

Kaolinization of 2:1 type clay minerals with different swelling properties

SHANGYING LI[1,2], HONGPING HE[1,2]*, QI TAO[1], JIANXI ZHU[1], WEI TAN[1], SHICHAO JI[1,2], YIPING YANG[1,2], AND CHAOQUN ZHANG[1,2]

[1] Key Laboratory of Mineralogy and Metallogeny, Chinese Academy of Sciences & Guangdong Provincial Key Laboratory of Mineral Physics and Materials, Guangzhou Institute of Geochemistry, Guangzhou 510640, China

[2] University of Chinese Academy of Sciences, Beijing 100049, China

* Corresponding author:
Prof. Hongping He
Present address:
Guangzhou Institute of Geochemistry,
Chinese Academy of Sciences,
No. 511 Kehua Street, Tianhe District, Guangzhou 510640, China.
E-mail address: hehp@gig.ac.cn

Always consult and cite the final, published document. See http:/www.minsocam.org or GeoscienceWorld

This is a preprint, the final version is subject to change, of the American Mineralogist (MSA)
Cite as Authors (Year) Title. American Mineralogist, in press.
DOI: https://doi.org/10.2138/am-2020-7339

ABSTRACT

Kaolinization of 2:1 type clay minerals commonly occurs in the supergene environments of the Earth, which plays critical roles in many geochemical and environmental processes. However, the transformation mechanism involved and the specific behavior of 2:1 type swelling and non-swelling clay minerals during kaolinization remain poorly understood. In this study, laboratory experiments on the kaolinization of montmorillonite (swelling), illite (non-swelling), and rectorite (partially swelling) were carried out to investigate the kaolinization mechanism of 2:1 type clay minerals and to evaluate whether swelling and non-swelling layers of 2:1 type clay minerals perform differently or not in their kaolinization processes. The results show that montmorillonite, illite, and rectorite in acidic Al^{3+}-containing solutions can be transformed into kaolinite, whereas such transformation is hard to take place in Al^{3+}-free solutions. Part of the Al^{3+} in the solutions was exchanged into the interlayer spaces of swelling clay minerals at the early stage and resulted in the formation of hydroxy-aluminosilicate (HAS) interlayers, but they show no influence on the transformation process. Interstratified kaolinite-smectite (K-S), kaolinite-illite (K-I), and kaolinite-rectorite (K-R) formed as the intermediate phases during the transformations of the three different precursor minerals, respectively. The results obtained in this study demonstrate that 2:1 type clay minerals, including both swelling and non-swelling ones, can be transformed into kaolinite via a local dissolution-crystallization mechanism, which starts mainly from the layer edges rather than the basal surfaces. Due to different dissolution rates from domain to domain

Always consult and cite the final, published document. See http:/www.minsocam.org or GeoscienceWorld

within a precursor mineral particle, the layers with a low dissolution rate become "splints", while the dissolved elements are concentrated between two "splints", leading to precipitation of kaolinite along the basal surfaces of precursor minerals. The size and stacking order of the newly formed kaolinite strongly depend on the morphology and property of the precursor minerals. These findings not only are of importance for better understanding the transformation procedures between different clay minerals and the mechanisms involved, but also provide new insights for well understanding mineral-water interactions that are central to all geochemical processes.

Keywords: Clay mineral, kaolinization, swelling property, dissolution-crystallization, mineral-water interaction

This is a preprint, the final version is subject to change, of the American Mineralogist (MSA)
Cite as Authors (Year) Title. American Mineralogist, in press.
DOI: https://doi.org/10.2138/am-2020-7339

INTRODUCTION

Transformation of 2:1 type phyllosilicates (e.g., montmorillonite and illite) into 1:1 type ones (e.g., kaolinite and halloysite) is ubiquitous in the supergene environments of the Earth (Karathanasis and Hajek, 1983; Singh and Gilkes, 1991; Kretzschmar et al., 1997; Amouric and Olives, 1998; Dong et al., 1998; Jolicoeur et al., 2000; Aspandiar and Eggleton, 2002; Dudek et al., 2006; Ryan and Huertas, 2009; Hong et al., 2015; Lu et al., 2016) and has been simulated under laboratory conditions (Cho and Komarneni, 2007; Dudek et al., 2007; Ryan and Huertas, 2013). Interstratified minerals, which are composed of layers with different chemical compositions and/or structures (Dudek et al., 2006; Hong et al., 2015), usually form as intermediate phases in transformation processes, whereas kaolinite and halloysite are commonly the end minerals of such transformations in tropical and subtropical areas (Hong et al., 2012; Ryan and Huertas, 2013). Understanding the transformation process and the mechanism involved is of great importance to unraveling the soil evolution and the climate change in the areas where such transformations occur (Karathanasis and Hajek, 1983; Kretzschmar et al., 1997; Aspandiar and Eggleton, 2002; Dudek et al., 2006; Ryan and Huertas, 2009, 2013; Hong et al., 2015). In addition, kaolinization of 2:1 type phyllosilicates closely relates to the migration and enrichment of rare earth elements (REE) in supergene environments (Bao and Zhao, 2008; Sanematsu et al., 2013), and kaolinite and halloysite have been considered as the main carriers for REE in the weathered crust elution-deposited REE deposits (Yang et al., 2019).

Always consult and cite the final, published document. See http:/www.minsocam.org or GeoscienceWorld

Transformations among various clay minerals can occur via two pathways: solid-state transformation (Amouric and Olives, 1998; Dudek et al., 2006; He et al., 2017; Ji et al., 2018) and dissolution-recrystallization (Środoń, 1980). The former refers to a transformation from a precursor mineral into other mineral phases in a solid-state by local rearrangement of atoms within the interlayer as the main route for atom diffusion in and out of the structure (Dudek et al., 2006; Lu et al., 2016; He et al., 2017; Ji et al., 2018), while dissolution-recrystallization usually occurs in systems with a high fluid/rock ratio, and involves complete dissolution of precursor minerals and subsequent recrystallization of other new phases (Dudek et al., 2006; Cuadros, 2012; Lu et al., 2016). In general, the solid-state transformation consumes less energy because, different from dissolution-recrystallization pathway, it does not require all of the chemical bonds in a precursor mineral to be broken. Solid-state transformation has been proposed as the most likely transformation mechanism for kaolinization of 2:1 type phyllosilicates, which could be realized by stripping one tetrahedral sheet from 2:1 type phyllosilicates and by preservation and adjustment of the other tetrahedral sheet and the octahedral sheet (Amouric and Olives, 1998; Dudek et al., 2006). Moreover, the formation of kaolinite-like patches within the smectite layers suggested that the kaolinization preferentially occurs in the internal regions rather than on the external surfaces (Dudek et al., 2006). However, external surfaces were also proposed to be the potential transformation sites because they are in direct contact with altering fluids (Dong et al., 1998). Thus, to better understand the transformation process and the mechanism involved, it is essential to determine whether kaolinization starts from

100 the external or internal surfaces (interlayers) of precursor minerals.

101 Field observations have shown that kaolinite and/or illite are the dominant clay
102 minerals in some bauxites and soils, whereas the content of smectite (e.g.,
103 montmorillonite and beidellite) is much lower than that of other 2:1 type clay
104 minerals (Calagari and Abedini, 2007; Liu et al., 2013; Yu et al., 2014; Ling et al.,
105 2017; Oliveira et al., 2018). As is well known, smectite belongs to swelling clay
106 minerals, whereas illite is a non-swelling one. For 2:1 type swelling clay minerals,
107 various cations and water molecules in solutions readily enter into their interlayer
108 spaces via cation exchange and/or diffusion. Consequently, both external and internal
109 surfaces are potential initiation sites of kaolinization, while external surfaces may be
110 the dominant transformation sites in the case of 2:1 type non-swelling clay minerals
111 (e.g., illite). This implies that the swelling property of 2:1 type clay minerals may
112 have a profound influence on their transformations. In other words, the kaolinization
113 of 2:1 type swelling clay minerals (e.g., smectite) may be more feasible than 2:1 type
114 non-swelling minerals (e.g., illite).

115 The primary aim of this study was therefore to investigate the kaolinization
116 processes of 2:1 type clay minerals with different swelling capacities, and to elucidate
117 the possible differences in their transformation behaviors and the mechanisms
118 involved. Three kinds of 2:1 type clay minerals with different swelling characteristics
119 were selected as starting minerals, i.e., montmorillonite (swelling), illite
120 (non-swelling), and rectorite (partially swelling), where rectorite is composed of
121 regularly interstratified illite-smectite (I-S) layers. The precursor minerals and their

kaolinization products were examined by X-ray diffraction (XRD), thermogravimetric analysis (TG), scanning electron microscopy (SEM), and high-resolution transmission electron microscopy (HRTEM). The results show that both 2:1 type swelling and non-swelling clay minerals can be transformed into kaolinite in acidic Al^{3+}-containing solutions. Such transformation realizes mainly via a local dissolution-crystallization pathway that starts from the layer edges rather than from the basal surfaces. The size and stacking order of the newly formed kaolinite strongly depend on the morphology and property of the precursor minerals. In the transformation procedures, part of free Al^{3+} in solutions can be exchanged into the interlayer spaces of 2:1 type swelling clay minerals, but they show no prominent influence on the kaolinization process.

MATERIALS AND METHODS

Starting materials

Three kinds of clay mineral samples, i.e., montmorillonite (Mnt), illite (Ill), and rectorite (Rec), were collected from the Inner Mongolia Autonomous Region, Zhejiang province, and Hubei province, China, respectively. Their chemical compositions were determined by using X-ray fluorescence spectroscopy (He et al., 2017) and shown in Table 1. To investigate the effect of interlayer cations on the transformation of montmorillonite, Al-exchanged montmorillonite (Al-Mnt) was prepared by exchanging interlayer Na^+ in the original Mnt with Al^{3+} from 1 M $AlCl_3$ solution for 12 h at ambient temperature. The cation exchange procedure was repeated twice, and the obtained sample was washed five times with deionized water to remove

144 redundant Al^{3+}. Our pre-experiments indicated that kaolinization of both the original
145 illite and rectorite with a large particle size was difficult to take place under the
146 hydrothermal conditions adopted in this study. Hence, the ground illite (G-Ill) and
147 ground rectorite (G-Rec) samples were prepared by ball-milling treatment of Ill and
148 Rec, respectively, and were used as the starting materials in the transformation
149 experiments. After ball-milling, the average size of illite grains decreased from ~1–2
150 μm in Ill to ~0.3–1 μm in G-Ill (Fig. 5a), and that of rectorite from ~0.5–1.5 μm in
151 Rec to ~0.3–1 μm in G-Rec (not shown). All the starting materials (Mnt, Al-Mnt, Ill,
152 G-Ill, and G-Rec) were of high purity, as indicated by their XRD patterns (Figs. 1, 4,
153 and 6). Aluminium chloride ($AlCl_3 \cdot 6H_2O$, analytical grade) was purchased from
154 Guangzhou Chemical Reagent Factory and was used to prepare the Al^{3+}-containing
155 solution (0.1 M) for hydrothermal experiments.

156 **Hydrothermal experiments**

157 The hydrothermal experiments for the transformation of 2:1 type clay minerals
158 into kaolinite were conducted as follows: 2 g of starting mineral was added to 80 ml
159 of Al^{3+}-containing solution under vigorous stirring, and the resultant suspension was
160 adjusted to a pH of 3 by adding concentrated hydrochloric acid. The obtained
161 suspension was transferred to a 250 ml *para*-phenylene lined autoclave, placed in an
162 oven, and then hydrothermally treated under the designed conditions with various
163 durations. All the experiments were carried out at 250°C under autogenous water
164 pressure.

165 The resultant products were washed with deionized water for five times and

centrifuged at 4000 r/min to remove redundant ions. The obtained products were dried at 80°C for 24 h and were labeled as Mnt-Al-X, Ill-Al-X, G-Ill-Al-X, and G-Rec-Al-X, respectively, where Al means that hydrothermal treatments were conducted in the acidic solutions containing Al^{3+} and X refers to the experiment duration. For example, Mnt-Al-8d denotes the product obtained in an acidic solution that contained Al^{3+} after 8-day hydrothermal treatment of Mnt. To evaluate the effect of Al^{3+} on the transformation, a control experiment without any free Al^{3+} in solution was conducted on Mnt under the identical hydrothermal condition, and the product was labeled as Mnt-8d. Meanwhile, a sample of Al-Mnt (Al-exchanged montmorillonite) was also treated under the identical condition as Mnt-8d, and the resulting product was labeled as Al-Mnt-8d.

Analytical techniques

X-ray diffraction (XRD). XRD measurements were performed on a Bruker D8 Advance diffractometer with Ni-filtered CuKα radiation (λ = 0.154 nm, 40 kV, and 40 mA). The XRD patterns of Mnt, Al-Mnt, Ill, and G-Ill and their hydrothermal products, were obtained between 3° and 45° (2θ), and those of G-Rec and its hydrothermal products were measured at 2° and 45° (2θ), with a scanning rate of 3° (2θ) min^{-1}.

Thermogravimetric analysis (TG). TG analyses were performed on a Netzsch STA 409PC instrument. Approximately 15 mg of ground sample was heated in a corundum crucible from 30 to 1000°C at a heating rate of 10°C min^{-1} under a pure N_2 atmosphere (60 cm^3/min) (He et al., 2017). The differential thermogravimetric (DTG)

188 curves were derived from the TG data.

189 **Scanning electron microscopy (SEM).** SEM images were obtained on a field
190 emission scanning electron microscope at 1.5 kV accelerating voltage and at a
191 working distance (WD) of 2.9 mm (FESEM, SU8010, Hitachi, Japan). Powder
192 samples were glued evenly onto conductive adhesive tapes for SEM observation.

193 **High-resolution transmission electron microscopy (HRTEM).** In order to
194 observe the lattice fringes of clay minerals along the [001] direction, oriented samples
195 were embedded in epoxy resin (Dong et al., 1998), and then dried at 100°C for 3 h.
196 Ultrathin (~75 nm) sections were then obtained using a diamond knife operated on a
197 Lecia EM UC7 ultramicrotome (Ji et al., 2018). The resulting section was placed on a
198 carbon-coated copper micro-grid for HRTEM observation. The HRTEM images were
199 obtained with a FEI Talos F200S microscope at an accelerating voltage of 200 kV.

200

201 # RESULTS

202 ## Transformation of montmorillonite

203 **XRD patterns.** The powder XRD patterns of Mnt and its hydrothermal products
204 with different duration time are shown in Figure 1. Montmorillonite is identified by
205 the series of characteristic reflections at ~1.23, ~0.45, and ~0.26 nm, corresponding to
206 (001), (02,11), and (13,20) reflections, respectively (Granquist and Pollack, 1967).
207 The d_{001} value (~1.23 nm) suggests that Na^+ is the dominant cation in the interlayer
208 space of montmorillonite, consistent with the chemical analysis result (Table 1).

209 In the case of the solution containing Al^{3+}, the basal spacing of montmorillonite

increases from 1.23 nm (Na-montmorillonite) to ~1.51 nm after a 1-day hydrothermal treatment (Fig. 1), resulting from the cation exchange of the interlayer Na^+ by Al^{3+} in solution. The (001) reflection of montmorillonite is dramatically broadened and weakened with an increase of the hydrothermal treatment time and almost disappears after an 8-day hydrothermal treatment (Fig. 1). This suggests a decrease in the stacking order of layers and/or the content of montmorillonite in the hydrothermal products. Note that two new reflections with *d*-values of ~0.72 and ~0.36 nm are recorded in the XRD patterns of the hydrothermal products (Fig. 1), corresponding to the (001) and (002) reflections of kaolinite, respectively (Dudek et al., 2006). The intensity of these two reflections gradually increases with an extension of hydrothermal reaction time, indicating an increase of the newly formed kaolinite content in the hydrothermal products. There are no reflections of kaolinite recorded between (130) (~0.26 nm) and (200) (~0.25 nm) reflections, and an almost overlapped reflection of $(1\bar{3}1)$ and (131) appears in 38–40° (2θ), reflecting that the newly formed kaolinite is highly disordered (Plancon et al., 1989).

In contrast, the hydrothermal products formed in the absence of Al^{3+} in solutions lack the reflections of kaolinite in their XRD patterns, whereas the reflections corresponding to montmorillonite remain almost unchanged (Fig. 1). The basal spacing of montmorillonite shifts to ~1.49 nm, which may be resulted from the intercalation of cations derived from micro-dissolved montmorillonite under the acidic conditions (Ryan and Huertas, 2013). In the case of Al-Mnt, the basal spacing is ~1.48 nm (Fig. 1), suggesting a successful exchange of Na^+ by Al^{3+} in the interlayer

space of the montmorillonite. After Al^{3+}-free hydrothermal treatment, the (001) reflection of montmorillonite becomes weak and broad, whereas no reflections of kaolinite are observed in Al-Mnt-8d (Fig. 1). These results suggest that montmorillonite is difficult to be transformed into kaolinite under hydrothermal solution conditions in the absence of Al^{3+}.

TG and DTG curves. TG and DTG curves of Mnt, Al-Mnt and their hydrothermal products are displayed in Figure 2, and the mass losses at different temperature ranges are summarized in Table 2. The mass loss of Mnt in the 30–300°C range corresponds to the dehydration of montmorillonite, whereas that at ~619°C is attributed to dehydroxylation (He et al., 2017). The mass loss of Mnt-Al-1d that corresponds to dehydration is about 17.52 wt%, which is significantly more than that of Mnt (10.46 wt%) (Fig. 2 and Table 2). This may be due to the two hydration shells of interlayer Al^{3+} cations in montmorillonite, different from the original Na-montmorillonite (Ryan and Huertas, 2013). Meanwhile, the dehydroxylation of montmorillonite in Mnt-Al-1d takes place at ~580°C, which is similar to that of Al-Mnt (Al-exchanged montmorillonite). The mass loss of dehydration gradually decreases with an extension of hydrothermal treatment time, whereas that of dehydroxylation increases (Table 2). The DTG curve of Mnt-Al-2d clearly displays two peaks centered at 484 and 570°C, respectively. This suggests that the product is a mixture of montmorillonite and newly formed kaolinite. A prominent mass loss of Mnt-Al-4d occurs at ~498°C, which is different from the dehydroxylation temperature of precursor montmorillonite but similar to that of kaolinite. In Mnt-Al-8d that is the

product after 8-day hydrothermal treatment, the two peaks of dehydration merge into one at ~84°C, whereas the dehydroxylation temperature is ~508°C. Our calculations show that the mass losses of dehydration is about 4.51 wt% and that of dehydroxylation is 11.05 wt% (Table 2), which are close to those of kaolinite rather than an interstratified K-S phase (Ryan and Huertas, 2013). These results suggest a complete transformation of montmorillonite into kaolinite occurring in Mnt-Al-8d.

SEM and HRTEM images. SEM observations show that montmorillonite in sample Mnt displays corrugated and scrolled morphology and the grain size is approximately 0.2–1 μm (Fig. 3a). Lattice fringes along the [001] direction of precursor montmorillonite usually display a periodicity of ~1.0 nm in the HRTEM image. The layer height of montmorillonite under HRTEM observations is slightly smaller than that indicated by XRD measurements (i.e., ~1.23 nm). This is due to the escape of interlayer water heated by the electron beam in the high vacuum circumstance (Fig. 3b). After hydrothermal treatment, the residual montmorillonite layers usually exhibit a periodicity of ~1.3 nm (Fig. 3b), suggesting that the formation of hydroxyl-Al polymers in the interlayer spaces of montmorillonite prevents the collapse of the layers to ~1.0 nm (Ryan and Huertas, 2009). The HRTEM images show that several lattice fringes with a periodicity of ~1.3 and ~0.7 nm, representing montmorillonite and kaolinite layers, respectively, are normal to the [001] direction (Fig. 3b). This indicates that an interstratified K-S phase formed during the kaolinization of montmorillonite. Note that the lattice fringe with a periodicity of ~0.7 nm is present between the thick lattice fringes of ~1.3 nm (Fig. 3b), which seems that

one kaolinite layer intercalated into the interlayer space of montmorillonite. This belongs to the denoted 0→K type of interstratified K-S structure (Amouric and Olives, 1998).

Transformation of illite

XRD patterns. The XRD pattern of Ill displays a sharp (001) reflection of illite at ~1.00 nm (Fig. 4). Different from the case of montmorillonite, there is no change of illite reflections after an 8-day hydrothermal treatment in acidic solutions with Al^{3+} (Fig. 4). This indicates that illite in Ill is stable and can hardly be transformed into kaolinite during the timescale of the experiment. However, boehmite was present in the hydrothermal product, as indicated by its characteristic reflection at 0.61 nm (Tsukada et al., 1999; Dudek et al., 2007).

After ball-milling, the reflection intensity of illite in G-Ill markedly decreases in comparison to that of the original illite (Fig. 4), which suggests a decrease of layer stacking order or crystallinity of illite. Sample G-Ill-Al-8d, the 8-day hydrothermal product of G-Ill, clearly exhibits the (001) reflection of kaolinite at ~0.72 nm, while the reflections of illite decrease in intensity (Fig. 4). This indicates that the product is a mixture of residual illite and newly formed kaolinite, as well as boehmite that is evidenced by the occurrence of the reflection at 0.61 nm.

SEM and HRTEM images. Lamellar illite grains with an average diameter of ~1–2 μm and euhedral morphology are displayed in the SEM image of Ill (Fig. 5a). After grinding (G-Ill), the size of illite particles decreases dramatically to ~0.3–1 μm with a subsequent increase of broken edges (Fig. 5a). The HRTEM image of sample

298 Ill shows that lattice fringes with a periodicity of ~1.0 nm parallelly stack along the
299 [001] direction of illite (Fig. 5b). After hydrothermal treatment, the presence of a
300 domain containing lattice fringes with a periodicity of ~0.7 nm indicates the presence
301 of newly formed kaolinite (Fig. 5b), consistent with the XRD result (Fig. 4). These
302 two kinds of lattice fringes also stack in parallel along the [001] direction (Fig. 5b),
303 which indicates the formation of interstratified kaolinite-illite (K-I).

304 **Transformation of rectorite**

305 **XRD patterns.** The (001) reflection of rectorite with a *d*-value of ~2.34 nm is
306 present in the XRD pattern of G-Rec, which is the sum of illite-like and
307 montmorillonite-like basal spacings (Fig. 6). With prolonged hydrothermal treatments,
308 the reflection intensity of rectorite decreases dramatically and eventually disappears
309 after an 8-day hydrothermal treatment, whereas that of kaolinite increases markedly
310 (Fig. 6). In particular, after an 8-day hydrothermal treatment (G-Rec-Al-8d), the (001)
311 reflection of kaolinite is sharp, and the reflections in the 2θ ranges of 20–22° and
312 38–40° are well resolved. This suggests that the crystallinity and layer stacking order
313 of newly formed kaolinite are higher than that of kaolinite in Mnt-Al-8d (Plancon et
314 al., 1989). In addition, the reflection occurring at ~0.61 nm also indicates the presence
315 of boehmite in the product (Fig. 6).

316 **HRTEM images.** Due to the escape of interlayer water from the
317 montmorillonite-like layers, the original rectorite usually exhibits lattice fringes with
318 a periodicity of ~2.0 nm along the [001] direction in the HRTEM images (Fig. 7).
319 However, residual rectorite in the hydrothermal product exhibits lattice fringes of

~2.3 nm periodicity (Fig. 7), which indicates the formation of hydroxy-Al polymers in the interlayer space of montmorillonite-like layers (Ryan and Huertas, 2009). An interstratified kaolinite-rectorite (K-R) phase is also observed, which simultaneously contains two kinds of nearly parallel lattice fringes with the periodicities of ~0.7 (kaolinite layer units) and ~2.3 nm (rectorite layer units) in the HRTEM image (Fig. 7). It is noteworthy that the kaolinite domains in the interstratified K-R usually contain a few lattice fringes with a periodicity of ~0.7 nm (Fig. 7), rather than prototypical kaolinite and montmorillonite/illite regular interstratified layers.

DISCUSSION

Effect of Al^{3+} in solution on kaolinization of 2:1 type clay minerals

Our results show that all of the 2:1 type clay minerals used (i.e., both swelling and non-swelling) can be successfully transformed into kaolinite in acidic solutions that contain Al^{3+} under hydrothermal conditions. However, our control experiments show that no kaolinite forms under the Al^{3+}-free hydrothermal condition (e.g., Mnt-8d) (Fig. 1). These results suggest that Al^{3+} in solutions plays a key role in the kaolinization of 2:1 type clay minerals (Dudek et al., 2007; Ryan and Huertas, 2013). With the presence of Al^{3+} in solutions, more protons can be generated by the hydrolysis of Al^{3+}, and subsequently, they can weaken tetrahedral-octahedral joint bonds or effectively break the oxygen atoms connecting the octahedral and tetrahedral sheets (Bickmore et al., 2001). Thus, the generated protons can greatly accelerate the decomposition of 2:1 type clay minerals. Meanwhile, the Al^{3+}-contained species

resulting from the hydrolysis of Al^{3+} can interact with Si dissolved from the 2:1 type clay minerals to form kaolinite, which can also promote the dissolution of precursor minerals.

Note that newly formed boehmite occurs in the hydrothermal products of Ill, G-Ill, and G-Rec, as indicated by the XRD patterns (Figs. 4 and 6), whereas boehmite was undetectable in the hydrothermal products from montmorillonite systems under the identical conditions (Fig. 1). This suggests that the behaviors of additive Al^{3+} in hydrothermal systems are closely related with the precursor clay minerals used. Such a difference in mineral components of the resulting hydrothermal products may be due to precursor minerals' various cation-exchange capacity as well as their swelling property. In the case of montmorillonite, part of the Al^{3+} in solution was readily able to enter into the interlayer spaces, which is identified by the d_{001} value of montmorillonite increasing to ~1.51 nm (Fig. 1) and the ~1.3 nm thick lattice fringes observed in the HRTEM images (Fig. 3b). For original rectorite, the HRTEM image exhibits lattice fringes with a periodicity of ~2.0 nm along the [001] direction (Fig. 7). The decrease of the unit layer thickness from ~2.34 nm (indicated by the XRD pattern in Fig. 6) to ~2.0 nm (indicated by the HRTEM image in Fig. 7) is attributed to the escape of interlayer water from the montmorillonite-like layers. However, the residual rectorite in the hydrothermal products exhibits lattice fringes of ~2.3 nm periodicity (Fig. 7), which suggests the entrance of Al^{3+} into the interlayer spaces of montmorillonite-like layers and the formation of hydroxy-Al polymers (Ryan and Huertas, 2009). These results indicate that Al^{3+} in solutions are readily to enter into

the interlayer spaces of 2:1 type swelling clay minerals during transformation. However, the height of illite layers remains unchanged before and after the hydrothermal reaction. This means that Al^{3+} in solutions was hard to enter into the interlayer spaces of 2:1 type non-swelling clay minerals and they readily form boehmite, as shown by the XRD patterns (Figs. 4 and 6).

Transformation procedures of 2:1 type swelling and non-swelling clay minerals into kaolinite

The reflections that correspond to montmorillonite almost completely disappear and the reflections of kaolinite are clearly recorded in the XRD pattern of the product after an 8-day hydrothermal treatment in the solution containing Al^{3+} (Mnt-Al-8d) (Fig. 1). This indicates a complete transformation of montmorillonite into kaolinite, consistent with the results of thermal analyses (Fig. 2 and Table 2). However, the reflections of illite are still detectable in the XRD patterns of sample Ill-Al-8d and G-Ill-Al-8d (Fig. 4). This reflects that montmorillonite is more readily transformed into kaolinite than illite under the identical conditions. Such a difference between the kaolinization of montmorillonite and illite maybe be attributed to their different layer charge density, interlayer cations as well as swelling property.

Both external and internal surfaces in montmorillonite are potential initiation sites for transformation taking place, while external surfaces are the dominant transformation sites in illite. To reveal the probable difference between kaolinization procedures of 2:1 type swelling (e.g., montmorillonite) and non-swelling (e.g., illite) clay minerals, it is of importance to determine their initial reaction sites in such

386 transformation, either in the interlayers (Dudek et al., 2006) and/or at the external
387 surfaces (e.g., edges) (Dong et al., 1998; Ma and Eggleton, 1999). The XRD pattern
388 of Al-Mnt-8d (Al-exchanged montmorillonite used as the precursor but without
389 additive Al^{3+} in solution) shows that there is no significant amount of kaolinite
390 occurring in the product when compared with sample Mnt-Al-8d (Na-montmorillonite
391 used as the precursor and with additive Al^{3+} in solution) in which a complete
392 kaolinization takes place (Fig. 1). This strongly suggests that the interlayer Al^{3+} does
393 not play a key role in the transformation of montmorillonite into kaolinite. In other
394 words, the internal surfaces are inert during the kaolinization of montmorillonite,
395 which implies that the transformation starts at the external surfaces (Dong et al.,
396 1998).

397 Illite is a typical 2:1 type non-swelling clay mineral with a large interlayer cation
398 (i.e., K^+) between adjacent layers. The interlayer K^+ is strongly electrostatically
399 attracted and is hardly replaced by other cations in solutions, which is confirmed by
400 the unchanged d_{001} value (~1.00 nm) before and after hydrothermal treatments (Fig. 4).
401 However, after ball-milling, illite in sample G-Ill is successfully transformed into
402 kaolinite as indicated by the XRD patterns and HRTEM images (Figs. 4 and 5b). As
403 shown by the SEM images of G-Ill (Fig. 5a), grinding treatment results in a dramatic
404 decrease of illite particle size, and particle edges become rough. Such changes make
405 the particle edges to be more feasible to react with protons in solution. As the
406 interlayer spaces of illite are fixed, kaolinization readily takes place at the edges rather
407 than in the interlayer spaces.

The initial reaction sites of the kaolinization of 2:1 type clay minerals are closely related to the dissolution zones of precursor minerals. The evidence from *in-situ* atomic force microscopy (AFM) observations showed that 2:1 type clay minerals (e.g., smectite) dissolved inward from their layer edges rather than their basal surfaces in both acidic (Bickmore et al., 2001) and alkaline (Kuwahara, 2006) environments. 2:1 type clay minerals with a larger proportion of broken edges would dissolve more quickly than others with "intact-edge", due to the existence of more coordinately unsaturated connecting oxygen atoms at these broken edges (Bickmore et al., 2001). This could reasonably explain the observation that ground illite, which has more broken edges (Fig. 5a) (Tao et al., 2014), is more easily to be transformed into kaolinite than non-ground illite under the identical condition as shown by their XRD patterns (Fig. 4). The difference in the kaolinization rate between montmorillonite and illite should also be related to the proportion of broken edges. In comparison to illite, montmorillonite always exhibits corrugated morphology and a smaller size (Figs. 3a and 5a). The latter corresponds to a larger proportion of broken edges, which is beneficial for the kaolinization of montmorillonite. Thus, illite and/or kaolinite, sometimes, can occur in bauxites and soils, whereas smectite is scarcely observed.

The above-mentioned proposal that kaolinization of 2:1 type clay minerals mainly starts at their edges can also well explain the 0→K type relationship between montmorillonite and kaolinite layers (i.e., a kaolinite layer is intercalated between two montmorillonite layers). It is well known that edge dislocations always occur within the particles of clay minerals, which have been observed as lattice fringe terminations

in HRTEM images (Ahn and Peacor, 1986; Murakami et al., 1999; Chen et al., 2013). Provided that the edge dislocation layer within a montmorillonite particle is transformed into a kaolinite layer from its edge, and its transformation rate is faster than that of adjacent layers, the kaolinite layer would form between two montmorillonite layers and terminate within the particle, leading to the formation of 0→K.

Rectorite is a regular interstratified I-S mineral with a 1:1 ratio of illite-like (non-swelling) and montmorillonite-like (swelling) layers. Thus, rectorite is an ideal mineral for revealing whether the swelling property of precursor minerals affects their kaolinization procedure or not. Provided that the swelling property has a prominent effect on kaolinization procedures of 2:1 type clay minerals, different transformation rates for montmorillonite-like and illite-like layers should be observed. In other words, the regular interstratified I-S layers may be probably transformed into regular interstratified I-K or K-S ones during the kaolinization of rectorite. However, our HRTEM images show that several consecutively stacked kaolinite layers occur within the interstratified K-R domains (Fig. 7), which suggests a transformation of rectorite layers into kaolinite layers rather than differentiated transformation between montmorillonite-like and illite-like layers. This implies that the swelling property of 2:1 type clay minerals has little influence on their kaolinization, and the transformation of rectorite into kaolinite corresponds to the dissolution of rectorite layers and subsequent crystallization of kaolinite.

In general, kaolinite formed via a complete dissolution-crystallization pathway

usually exhibits different crystallographic orientations with respect to those of precursor minerals due to the diffusion and transport of chemical components in solution (Cuadros, 2012). However, our HRTEM images of the intermediate phases (e.g., interstratified K-S, K-I, and K-R) show that the residual precursor mineral layers (i.e., montmorillonite, illite, and rectorite) and the newly formed kaolinite layers are parallel to each other along the [001] direction (Figs. 3b, 5b, and 7). Such inheritance of crystallographic orientation is closely related to an interface-coupled dissolution-precipitation pathway in which structural matching between precursors and newly formed minerals is a prerequisite (Putnis, 2014). The *in-situ* AFM observations have demonstrated that dissolution of 2:1 type clay minerals starts from their layer edges and goes inward with an extension of time (Bickmore et al., 2001; Kuwahara, 2006). However, due to the heterogeneity in chemical components and crystal defects, different dissolution rates from layer (i.e., domain) to layer within a precursor mineral particle can occur in the transformation procedure, as demonstrated by the HRTEM images of hydrothermal products in the present study (Figs. 3b, 5b, and 7). Thus, the layers with a low dissolution rate will become "splints" while the dissolved elements (e.g., Si and Al) from precursor minerals are concentrated between two "splints", leading to precipitation of kaolinite along the basal surfaces of precursor minerals. Such a kaolinization model (i.e., local dissolution-crystallization) is different from that proposed by Dudek et al. (2006), in which the kaolinization of smectite is realized by stripping of the tetrahedral sheets from the internal surfaces of precursor minerals. Meanwhile, the excess of Si dissolved from 2:1 type clay minerals

474 can react with additive Al^{3+} in solution to form kaolinite via a complete
475 dissolution-crystallization pathway. Hence, the transformation procedure observed in
476 this study can be depicted by using Figure 8, in which both local
477 dissolution-crystallization (LDC) and complete dissolution-crystallization (CDC) are
478 proposed to take place in the kaolinization procedure.

479 As shown by the HRTEM images (Figs. 3b and 5b), kaolinite in G-Ill-Al-8d
480 displays relatively larger size and highly ordered stacking along the *c* axis with
481 respect to that of kaolinite in Mnt-Al-8d. Such difference also closely relates with
482 particle size and morphology of the precursor minerals. In the case of illite, its larger
483 particle size leads to bigger two-dimensional and confined spaces with residual
484 aluminosilicates dissolved from precursor minerals, followed by the formation of
485 highly ordered kaolinite with a larger size. In contrast, for montmorillonite, due to its
486 smaller size and corrugated morphology, the resulting kaolinite via local
487 dissolution-crystallization is usually in small size and with poor stacking order.
488 Similar morphology and structure are also observed in the kaolinite transformed from
489 rectorite (Figs. 6 and 7). These observations suggest that the size and stacking order of
490 the newly formed kaolinite strongly depend on the morphology and property of the
491 precursor minerals.

492

493 **IMPLICATIONS**

494 Clay minerals are ubiquitous in various geological environments on the Earth's
495 surface where the interaction between aqueous solutions and solids as well as the

coupled dissolution-precipitation of minerals are very active (Putnis, 2014). However, the transformations among various clay minerals dominated by a local dissolution-crystallization pathway are rarely reported. Due to small particle size and various morphologies of clay minerals, it is difficult to obtain microscopic evidence from such transformation processes. The present study suggests that the formation of interstratified minerals during kaolinization of 2:1 type clay minerals involves two basic steps: dissolution of precursor minerals, and subsequent crystallization of kaolinite in the two-dimensional and confined spaces resulted from the different dissolution rates of precursor mineral layers, i.e., local dissolution-crystallization. In general, the new phases formed by a local dissolution-crystallization pathway will incompletely cover the substrate surfaces of precursor minerals for continuous transformation reactions (Putnis, 2014). However, the present study shows that, in the case of the transformation of 2:1 type clay minerals into kaolinite, the dissolution of 2:1 type clay minerals starts mainly from the layer edges, whereas the subsequent crystallization of kaolinite takes place on the basal surfaces of precursor minerals. This is different from three-dimensional minerals (Putnis, 2014). In natural open systems such as weathering profiles, the dissolution of 2:1 type phyllosilicates (e.g., muscovite) and the subsequent crystallization of 1:1 type clay minerals at the edges of precursor minerals are also observed (Lu et al., 2016). This suggests that the local environment in which the mineral-water interactions take place is a key factor in controlling reaction pathways and mechanisms involved.

As demonstrated by the present study, local dissolution-crystallization is a

518 dominant pathway for the transformation of 2:1 type clay minerals into kaolinite.
519 Local dissolution of precursor clay minerals (e.g., montmorillonite) can generate HAS
520 interlayers prior to the formation of kaolinite, which suggests that HAS containing 2:1
521 type clay minerals may be the product at the beginning stage of the transformation of
522 2:1 type clay minerals into 1:1 type ones. This is obviously different from the
523 previous proposal that HAS interlayers form through the adsorption of HAS ions into
524 the interlayer spaces of 2:1 type clay minerals in the acidic condition (Lou and Huang,
525 1988), and provides insight for better understanding the occurrence of HAS
526 containing 2:1 type clay minerals in nature.
527

528 **ACKNOWLEDGMENTS**

529 This work was financially supported by National Natural Science Foundation of
530 China (Grant Nos.41530313, 41772039), National Science Fund for Distinguished
531 Young Scholars of China (Grant No.41825003), and CAS Key Research Program of
532 Frontier Sciences (Grant No. QYZDJ-SSW-DQC023-1). The authors thank Warren
533 Huff for handling this paper, and the anonymous reviewers for their valuable
534 comments and suggestions.
535

REFERENCES CITED

Ahn, J.H., and Peacor, D.R. (1986) Transmission electron-microscope data for rectorite: Implications for the origin and structure of "Fundamental particles". Clays and Clay Minerals, 34, 180-186.

Amouric, M., and Olives, J. (1998) Transformation mechanisms and interstratification in conversion of smectite to kaolinite: An HRTEM study. Clays and Clay Minerals, 46, 521-527.

Aspandiar, M.F., and Eggleton, R.A. (2002) Weathering of chlorite: I. Reactions and products in microsystems controlled by the primary mineral. Clays and Clay Minerals, 50, 685-698.

Bao, Z.W., and Zhao, Z.H. (2008) Geochemistry of mineralization with exchangeable REY in the weathering crusts of granitic rocks in South China. Ore Geology Reviews, 33, 519-535.

Bickmore, B.R., Bosbach, D., Hochella, M.F., Charlet, L., and Rufe, E. (2001) In situ atomic force microscopy study of hectorite and nontronite dissolution: Implications for phyllosilicate edge surface structures and dissolution mechanisms. American Mineralogist, 86, 411-423.

Calagari, A.A., and Abedini, A. (2007) Geochemical investigations on Permo-Triassic bauxite horizon at Kanisheeteh, east of Bukan, West-Azarbaidjan, Iran. Journal of Geochemical Exploration, 94, 1-18.

Chen, T., Wang, H.J., Li, T., and Zheng, N. (2013) New insights into the formation of diagenetic illite from TEM studies. American Mineralogist, 98, 879-887.

558 Cho, Y.C., and Komarneni, S. (2007) Synthesis of kaolinite from micas and
559 K-depleted micas. Clays and Clay Minerals, 55, 565-571.
560 Cuadros, J. (2012) Clay crystal-chemical adaptability and transformation
561 mechanisms. Clay Minerals, 47, 147-164.
562 Dong, H.L., Peacor, D.R., and Murphy, S.F. (1998) TEM study of progressive
563 alteration of igneous biotite to kaolinite throughout a weathered soil profile.
564 Geochimica et Cosmochimica Acta, 62, 1881-1887.
565 Dudek, T., Cuadros, J., and Fiore, S. (2006) Interstratified kaolinite-smectite: Nature
566 of the layers and mechanism of smectite kaolinization. American Mineralogist,
567 91, 159-170.
568 Dudek, T., Cuadros, J., and Huertas, J. (2007) Structure of mixed-layer
569 kaolinite-smectite and smectite-to-kaolinite transformation mechanism from
570 synthesis experiments. American Mineralogist, 92, 179-192.
571 Granquist, W.T., and Pollack, S.S. (1967) Clay mineral synthesis. Ⅱ. A randomly
572 interstratified aluminian montmorillonoid. American Mineralogist, 52, 212-226.
573 He, H.P., Ji, S.C., Tao, Q., Zhu, J.X., Chen, T.H., Liang, X.L., Li, Z.H., and Dong,
574 H.L. (2017) Transformation of halloysite and kaolinite into beidellite under
575 hydrothermal condition. American Mineralogist, 102, 997-1005.
576 Hong, H.L., Cheng, F., Yin, K., Churchman, G.J., and Wang, C.W. (2015)
577 Three-component mixed-layer illite/smectite/kaolinite (I/S/K) minerals in
578 hydromorphic soils, south China. American Mineralogist, 100, 1883-1891.
579 Hong, H.L., Churchman, G.J., Gu, Y.S., Yin, K., and Wang, C.W. (2012)

580 Kaolinite-smectite mixed-layer clays in the Jiujiang red soils and their climate
581 significance. Geoderma, 173, 75-83.
582 Ji, S.C., Zhu, J.X., He, H.P., Tao, Q., Zhu, R.L., Ma, L.Y., Chen, M., Li, S.Y., and
583 Zhou, J.M. (2018) Conversion of serpentine to smectite under hydrothermal
584 condition: Implication for solid-state transformation. American Mineralogist.
585 103, 241-251.
586 Jolicoeur, S., Ildefonse, P., and Bouchard, M. (2000) Kaolinite and gibbsite
587 weathering of biotite within saprolites and soils of central Virginia. Soil Science
588 Society of America Journal, 64, 1118-1129.
589 Karathanasis, A.D., and Hajek, B.F. (1983) Transformation of smectite to kaolinite in
590 naturally acid soil systems-structural and thermodynamic considerations. Soil
591 Science Society of America Journal, 47, 158-163.
592 Kretzschmar, R., Robarge, W.P., Amoozegar, A., and Vepraskas, M.J. (1997) Biotite
593 alteration to halloysite and kaolinite in soil-saprolite profiles developed from
594 mica schist and granite gneiss. Geoderma, 75, 155-170.
595 Kuwahara, Y. (2006) In-situ AFM study of smectite dissolution under alkaline
596 conditions at room temperature. American Mineralogist, 91, 1142-1149.
597 Ling, K.Y., Zhu, X.Q., Tang, H.S., and Li, S.X. (2017) Importance of
598 hydrogeological conditions during formation of the karstic bauxite deposits,
599 Central Guizhou Province, Southwest China: A case study at Lindai deposit. Ore
600 Geology Reviews, 82, 198-216.
601 Liu, X.F., Wang, Q.F., Feng, Y.W., Li, Z.M., and Cai, S.H. (2013) Genesis of the

602 Guangou karstic bauxite deposit in western Henan, China. Ore Geology Reviews,
603 55, 162-175.
604 Lou, G., and Huang, P.M. (1988) Hydroxy-aluminosilicate interlayers in
605 montmorillonite - implications for acidic environments. Nature, 335, 625-627.
606 Lu, Y.Q., Wang, R.C., Lu, X.C., Li, J., and Wang, T.T. (2016) Reprint of genesis of
607 halloysite from the weathering of muscovite: Insights from microscopic
608 observations of a weathered granite in the Gaoling Area, Jingdezhen, China.
609 Applied Clay Science, 119, 59-66.
610 Ma, C., and Eggleton, R.A. (1999) Surface layer types of kaolinite: A high-resolution
611 transmission electron microscope study. Clays and Clay Minerals, 47, 181-191.
612 Murakami, T., Sato, T., and Inoue, A. (1999) HRTEM evidence for the process and
613 mechanism of saponite-to-chlorite conversion through corrensite. American
614 Mineralogist, 84, 1080-1087.
615 Oliveira, D.P., Sartor, L.R., Souza, V.S., Correa, M.M., Romero, R.E., Andrade,
616 G.R.P., and Ferreira, T.O. (2018) Weathering and clay formation in semi-arid
617 calcareous soils from Northeastern Brazil. Catena, 162, 325-332.
618 Plancon, A., Giese, R.F., Snyder, R., Drits, V.A., and Bookin, A.S. (1989)
619 Stacking-faults in the kaolin-group minerals-defect structures of kaolinite. Clays
620 and Clay Minerals, 37, 203-210.
621 Putnis, A. (2014) Why mineral interfaces matter. Science, 343, 1441-1442.
622 Ryan, P.C., and Huertas, F.J. (2009) The temporal evolution of pedogenic Fe-smectite
623 to Fe-kaolin via interstratified kaolin-smectite in a moist tropical soil

chronosequence. Geoderma, 151, 1-15.

Ryan, P.C., and Huertas, F.J. (2013) Reaction pathways of clay minerals in tropical soils: insights from kaolinite-smectite synthesis experiments. Clays and Clay Minerals, 61, 303-318.

Sanematsu, K., Kon, Y., Imai, A., Watanabe, K., and Watanabe, Y. (2013) Geochemical and mineralogical characteristics of ion-adsorption type REE mineralization in Phuket, Thailand. Mineralium Deposita, 48, 437-451.

Singh, B., and Gilkes, R.J. (1991) Weathering of a chromian muscovite to kaolinite. Clays and Clay Minerals, 39, 571-579.

Środoń, J. (1980) Synthesis of mixed-layer kaolinite-smectite. Clays and Clay Minerals, 28, 419-424.

Tao, Q., Su, L., Frost, R.L., Zhang, D., Chen, M., Shen, W., and He, H. (2014) Silylation of mechanically ground kaolinite. Clay Minerals, 49, 559-568.

Tsukada, T., Segawa, H., Yasumori, A., and Okada, K. (1999) Crystallinity of boehmite and its effect on the phase transition temperature of alumina. Journal of Materials Chemistry, 9, 549-553.

Yang, M.J., Liang, X.L., Ma, L.Y., Hang, J., He, H.P., and Zhu, J.X. (2019) Adsorption of REEs on kaolinite and halloysite: A link to the REE distribution on clays in the weathering crust of granite. Chemical Geology, 525, 210-217.

Yu, W.C., Wang, R.H., Zhang, Q.L., Du, Y.S., Chen, Y., and Liang, Y.P. (2014) Mineralogical and geochemical evolution of the Fusui bauxite deposit in Guangxi, South China: From the original Permian orebody to a Quarternary

This is a preprint, the final version is subject to change, of the American Mineralogist (MSA)
Cite as Authors (Year) Title. American Mineralogist, in press.
DOI: https://doi.org/10.2138/am-2020-7339

Salento-type deposit. Journal of Geochemical Exploration, 146, 75-88.

Always consult and cite the final, published document. See http:/www.minsocam.org or GeoscienceWorld

This is a preprint, the final version is subject to change, of the American Mineralogist (MSA)
Cite as Authors (Year) Title. American Mineralogist, in press.
DOI: https://doi.org/10.2138/am-2020-7339

FIGURE CAPTIONS

FIGURE 1. XRD patterns of samples of Mnt and Al-Mnt and their hydrothermal products. Hydrothermal products obtained from Mnt treated with acidic solutions containing Al^{3+} after 1 day (Mnt-Al-1d), 2 days (Mnt-Al-2d), 4 days (Mnt-Al-4d), and 8 days (Mnt-Al-8d). Hydrothermal product obtained from acidic solution after 8 days of using Mnt as starting material (Mnt-8d), and that obtained from using Al-Mnt as starting material (Al-Mnt-8d). M: montmorillonite; Q: quartz; C: calcite; K: kaolinite. All spacing units are in nanometers (nm).

FIGURE 2. TG and DTG curves of Mnt and its hydrothermal products, as well as of Al-Mnt. Hydrothermal products obtained from acidic solutions containing Al^{3+} after 1 day (Mnt-Al-1d), 2 days (Mnt-Al-2d), 4 days (Mnt-Al-4d), and 8 days (Mnt-Al-8d).

FIGURE 3. SEM image (a) of sample Mnt and HRTEM images (b) of sample Mnt and its hydrothermal products. Hydrothermal product obtained from acidic solutions containing Al^{3+} after 2 days (Mnt-Al-2d), and 4 days (Mnt-Al-4d). Large arrow indicates the [001] direction of clay minerals.

FIGURE 4. XRD patterns of sample Ill and G-Ill and their hydrothermal products. Hydrothermal product obtained from acidic solution containing Al^{3+} after 8 days, with Ill as a starting material (Ill-Al-8d), and with G-Ill as starting material (G-Ill-Al-8d). I: illite; K: kaolinite; B: boehmite; C: corundum. All spacing units are in nanometers

Always consult and cite the final, published document. See http:/www.minsocam.org or GeoscienceWorld

(nm).

FIGURE 5. SEM images (a) of sample Ill and G-Ill and HRTEM images (b) of G-Ill and its hydrothermal product. Hydrothermal product obtained from acidic solution containing Al^{3+} after 8 days, with G-Ill as the starting material (G-Ill-Al-8d). Large arrow indicates the [001] direction of clay minerals.

FIGURE 6. XRD patterns of sample G-Rec and its hydrothermal products. Hydrothermal products obtained from acidic solution containing Al^{3+} after 2 days (G-Rec-Al-2d), 4 days (G-Rec-Al-4d), and 8 days (G-Rec-Al-8d). R: rectorite; K: kaolinite; B: boehmite. All spacing units are in nanometers (nm).

FIGURE 7. HRTEM image of sample G-Rec and its hydrothermal product. Hydrothermal product obtained from acidic solution containing Al^{3+} after 2 days (G-Rec-Al-2d). Large arrow indicates the [001] direction of clay minerals.

FIGURE 8. Schematic representation of the transformation of 2:1 type clay mineral into kaolinite in acidic solution containing Al^{3+}. (a) original 2:1 type clay mineral; (b) layer of original 2:1 type clay mineral dissolving from its edges; (c) kaolinite layer formed by local dissolution-crystallization, and interstratified mineral. LDC-K denotes kaolinite layer formed by local dissolution-crystallization. CDC-K denotes kaolinite layer formed by complete dissolution-crystallization.

This is a preprint, the final version is subject to change, of the American Mineralogist (MSA)
Cite as Authors (Year) Title. American Mineralogist, in press.
DOI: https://doi.org/10.2138/am-2020-7339

694 # TABLES

695 **TABLE 1.** Chemical compositions of starting materials.

	Al_2O_3	CaO	Fe_2O_3	K_2O	MgO	Na_2O	P_2O_5	SiO_2	TiO_2	H_2O	Total(%)
Mnt	15.98	2.94	4.86	0.21	4.98	3.21	0.03	59.40	0.32	7.88	99.81
Ill	36.60	0.22	0.25	9.57	0.24	0.25	0.20	47.12	0.41	4.83	99.70
Rec	34.49	5.25	0.43	0.79	0.33	1.40	2.26	41.75	4.23	8.28	99.21

696 The values in Table 1 were obtained by measuring parallel samples and their relative
697 standard deviations were less than 2.25 %.

698

699 **TABLE 2.** Mass losses of dehydrations and dehydroxylations of sample Mnt and its
700 hydrothermal products obtained from acidic solutions containing Al^{3+} after different
701 durations and those of sample Al-Mnt.

Samples	Dehydration (wt%)	Dehydroxylation (wt%)	Mnt/%[a]	Kao/%[b]
	(30-300°C)	(300-800°C)		
Mnt	10.46	6.32	100.00	0.00
Mnt-Al-1d	17.52	4.78	89.34	9.14
Mnt-Al-2d	13.85	6.41	64.46	33.39
Mnt-Al-4d	8.41	8.87	27.48	69.78
Mnt-Al-8d	4.51	11.05	0.00	100.00
Al-Mnt	19.15	4.22	100.00	0.00

702 [a] Relative content of montmorillonite layers in clay minerals in each sample; [b]
703 Relative content of kaolinite layers. Here, it is assumed relative contents of

Always consult and cite the final, published document. See http:/www.minsocam.org or GeoscienceWorld

This is a preprint, the final version is subject to change, of the American Mineralogist (MSA)
Cite as Authors (Year) Title. American Mineralogist, in press.
DOI: https://doi.org/10.2138/am-2020-7339

montmorillonite and kaolinite layers in clay minerals are 100.00 % in Al-Mnt and Mnt-Al-8d, respectively, based on XRD patterns in Fig 1. Relative contents of montmorillonite and kaolinite layers in other hydrothermal products were calculated from mass losses of hydrations and dehydrations of sample Al-Mnt (not Mnt) and Mnt-Al-8d, due to different hydration interlayer states of montmorillonite before (Na-montmorillonite) and after hydrothermal treatment (Al-montmorillonite).

Always consult and cite the final, published document. See http:/www.minsocam.org or GeoscienceWorld

This is a preprint, the final version is subject to change, of the American Mineralogist (MSA)
Cite as Authors (Year) Title. American Mineralogist, in press.
DOI: https://doi.org/10.2138/am-2020-7339

Figure 1

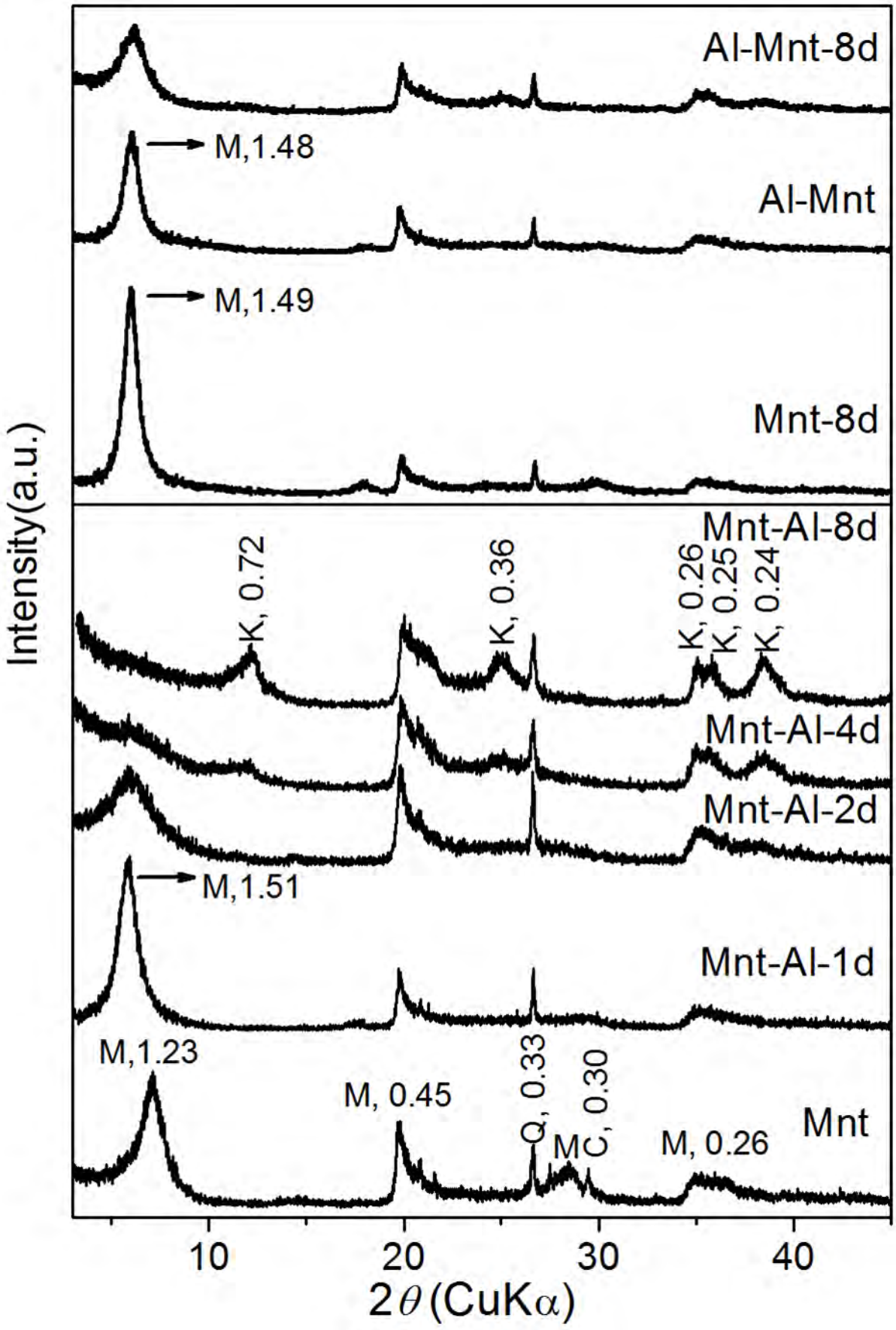

Always consult and cite the final, published document. See http:/www.minsocam.org or GeoscienceWorld

This is a preprint, the final version is subject to change, of the American Mineralogist (MSA)
Cite as Authors (Year) Title. American Mineralogist, in press.
DOI: https://doi.org/10.2138/am-2020-7339

Figure 2

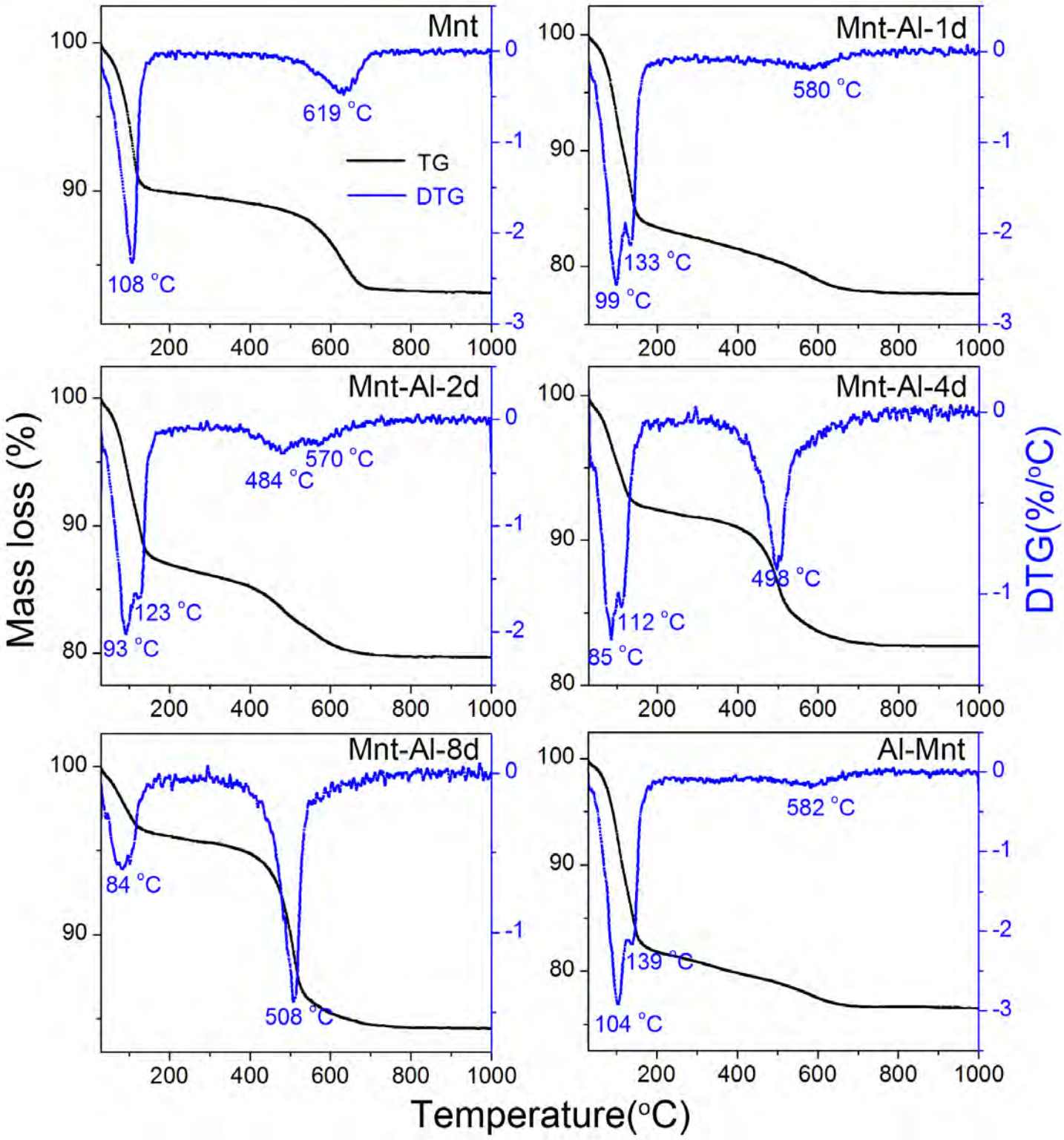

Always consult and cite the final, published document. See http:/www.minsocam.org or GeoscienceWorld

This is a preprint, the final version is subject to change, of the American Mineralogist (MSA)
Cite as Authors (Year) Title. American Mineralogist, in press.
DOI: https://doi.org/10.2138/am-2020-7339

Figure 3

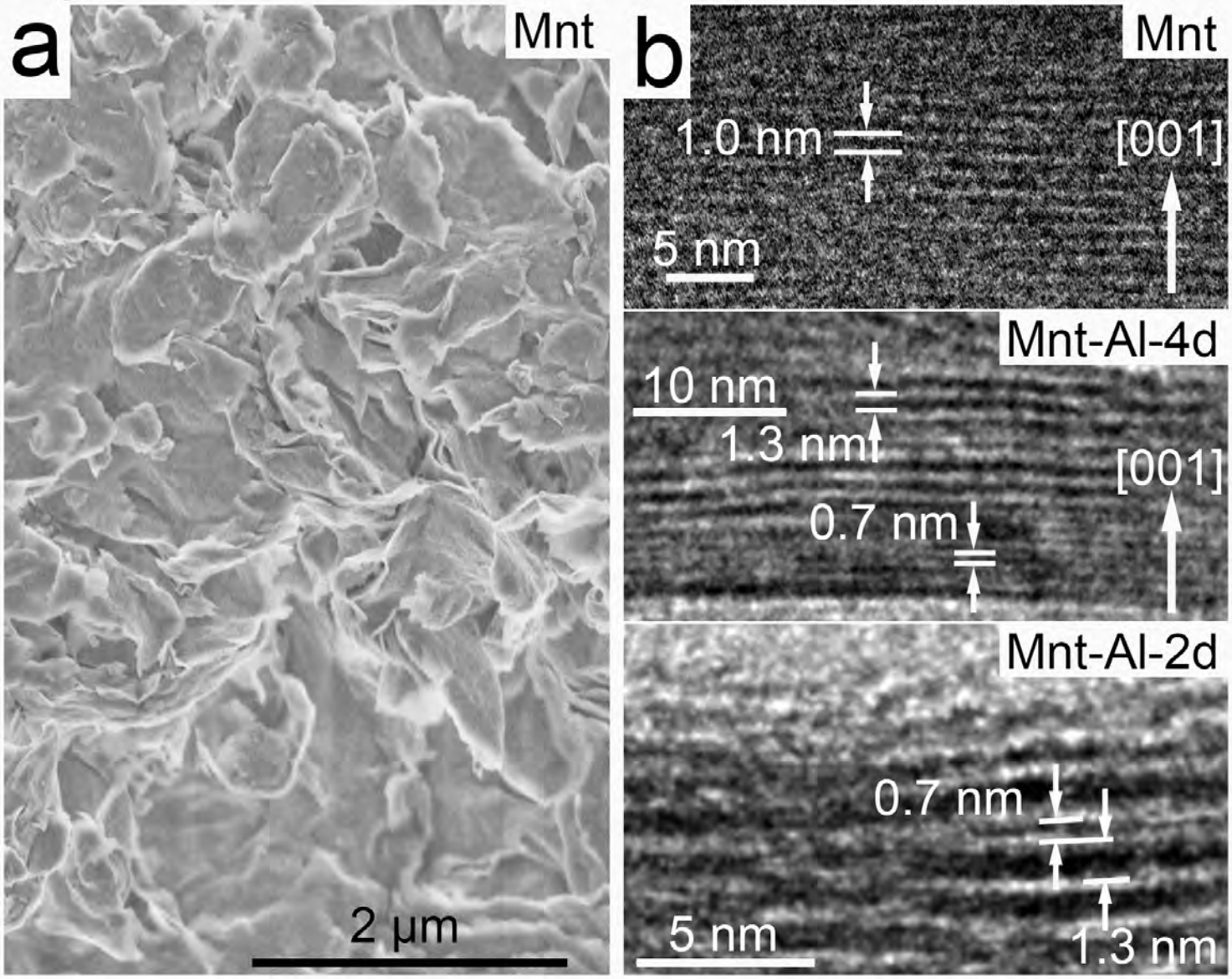

Always consult and cite the final, published document. See http:/www.minsocam.org or GeoscienceWorld

This is a preprint, the final version is subject to change, of the American Mineralogist (MSA)
Cite as Authors (Year) Title. American Mineralogist, in press.
DOI: https://doi.org/10.2138/am-2020-7339

Figure 4

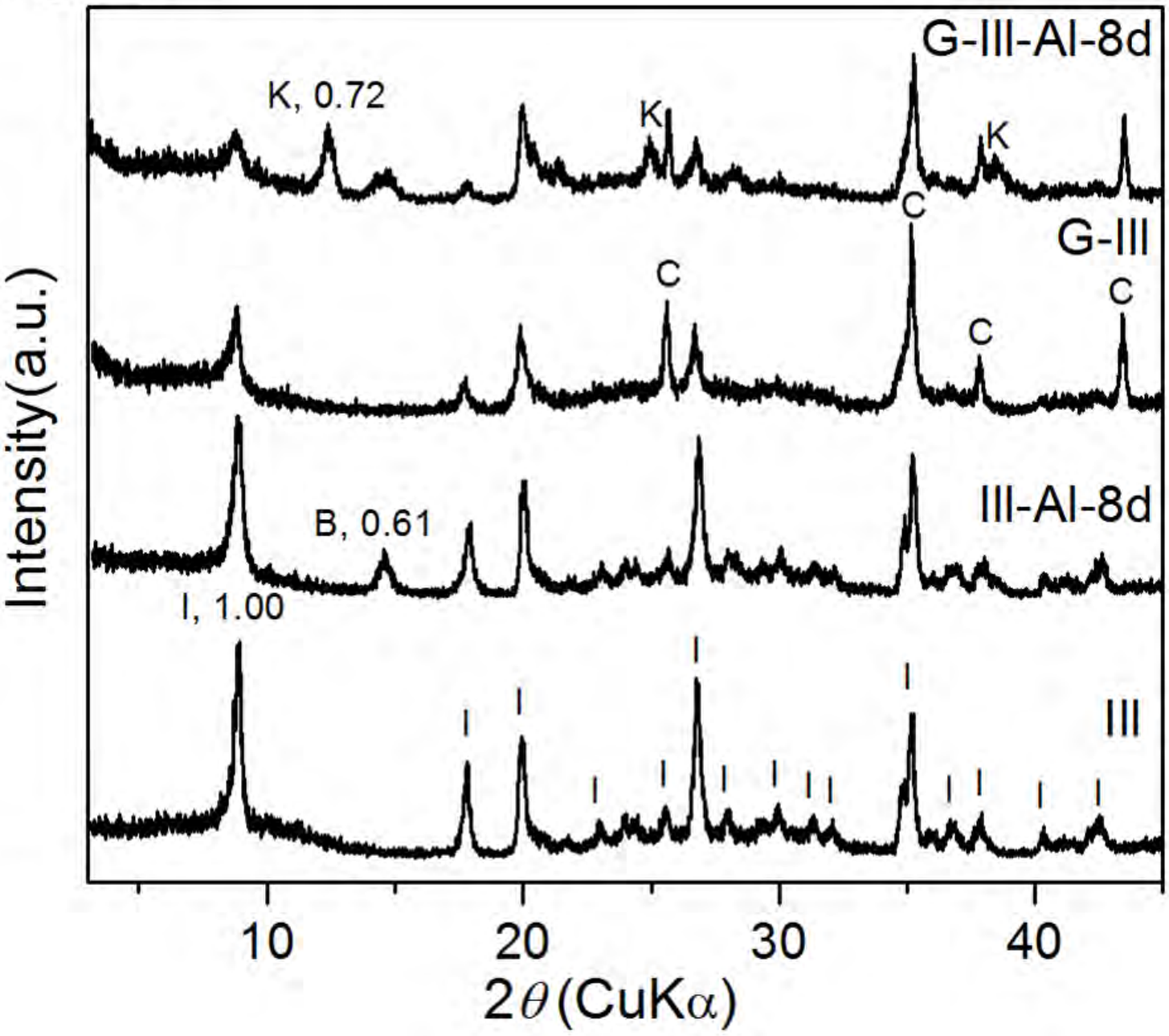

Always consult and cite the final, published document. See http:/www.minsocam.org or GeoscienceWorld

This is a preprint, the final version is subject to change, of the American Mineralogist (MSA)
Cite as Authors (Year) Title. American Mineralogist, in press.
DOI: https://doi.org/10.2138/am-2020-7339

Figure 5

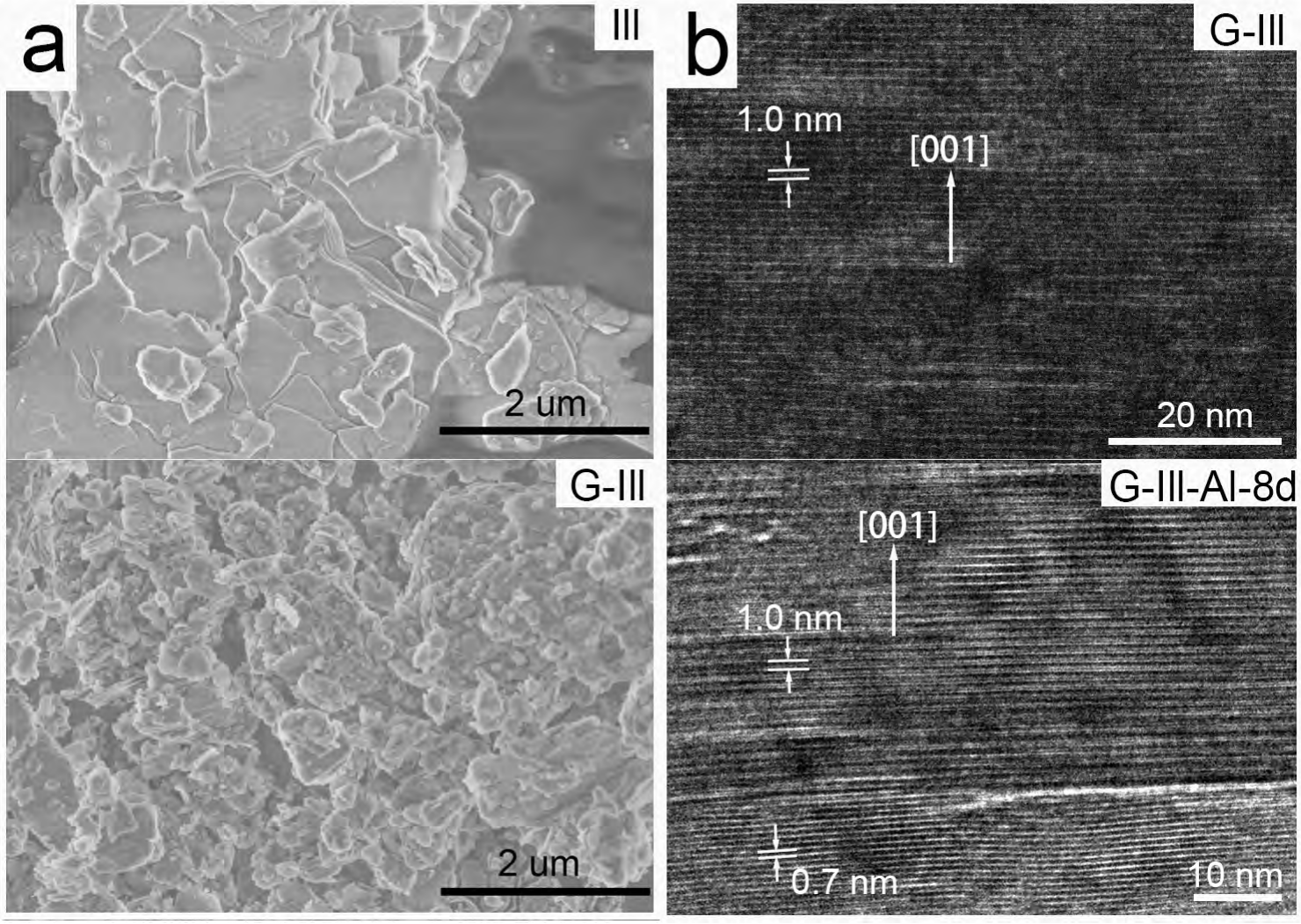

Always consult and cite the final, published document. See http:/www.minsocam.org or GeoscienceWorld

This is a preprint, the final version is subject to change, of the American Mineralogist (MSA)
Cite as Authors (Year) Title. American Mineralogist, in press.
DOI: https://doi.org/10.2138/am-2020-7339

Figure 6

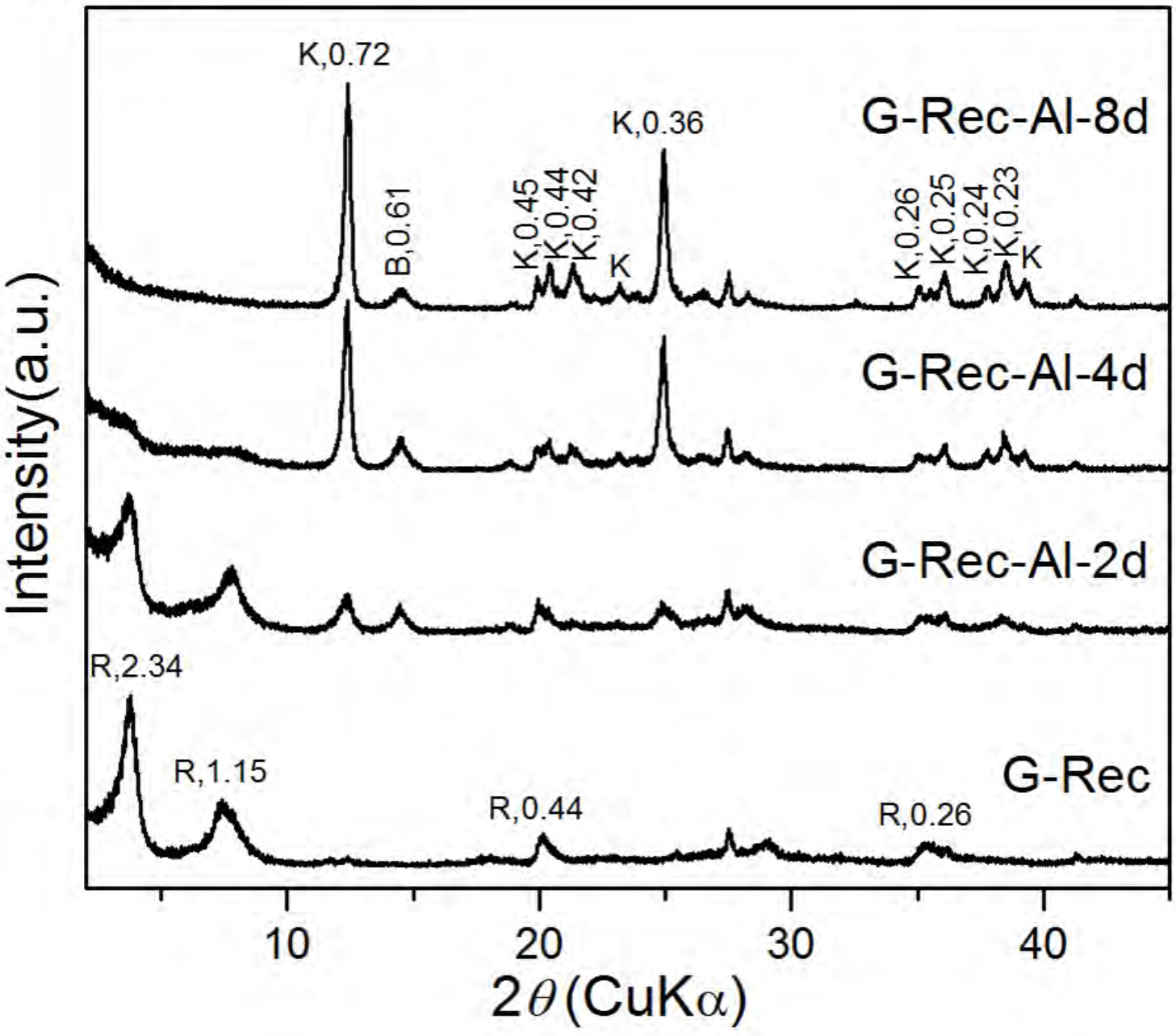

Always consult and cite the final, published document. See http:/www.minsocam.org or GeoscienceWorld

This is a preprint, the final version is subject to change, of the American Mineralogist (MSA)
Cite as Authors (Year) Title. American Mineralogist, in press.
DOI: https://doi.org/10.2138/am-2020-7339

Figure 7

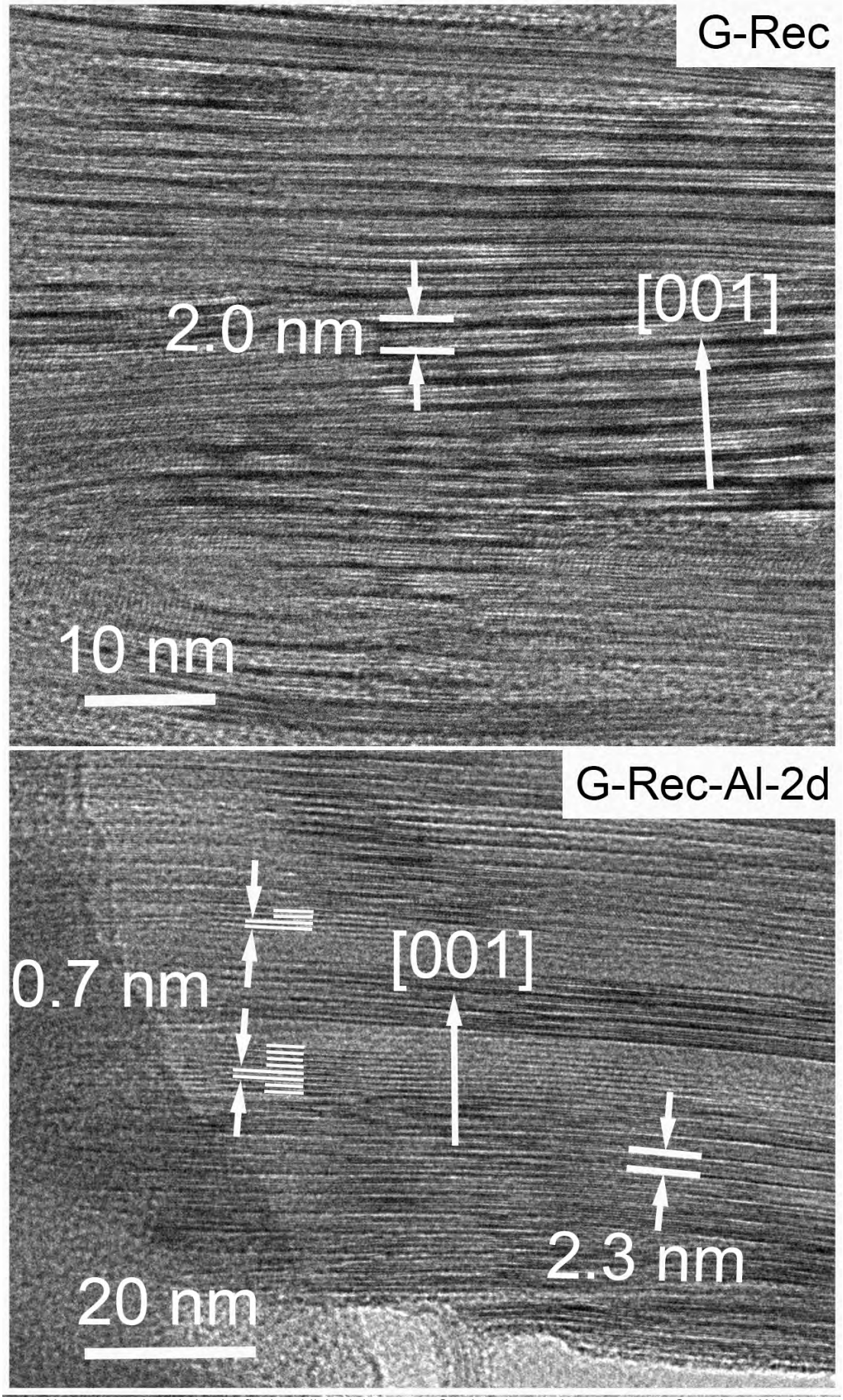

Always consult and cite the final, published document. See http:/www.minsocam.org or GeoscienceWorld

This is a preprint, the final version is subject to change, of the American Mineralogist (MSA)
Cite as Authors (Year) Title. American Mineralogist, in press.
DOI: https://doi.org/10.2138/am-2020-7339

Figure 8

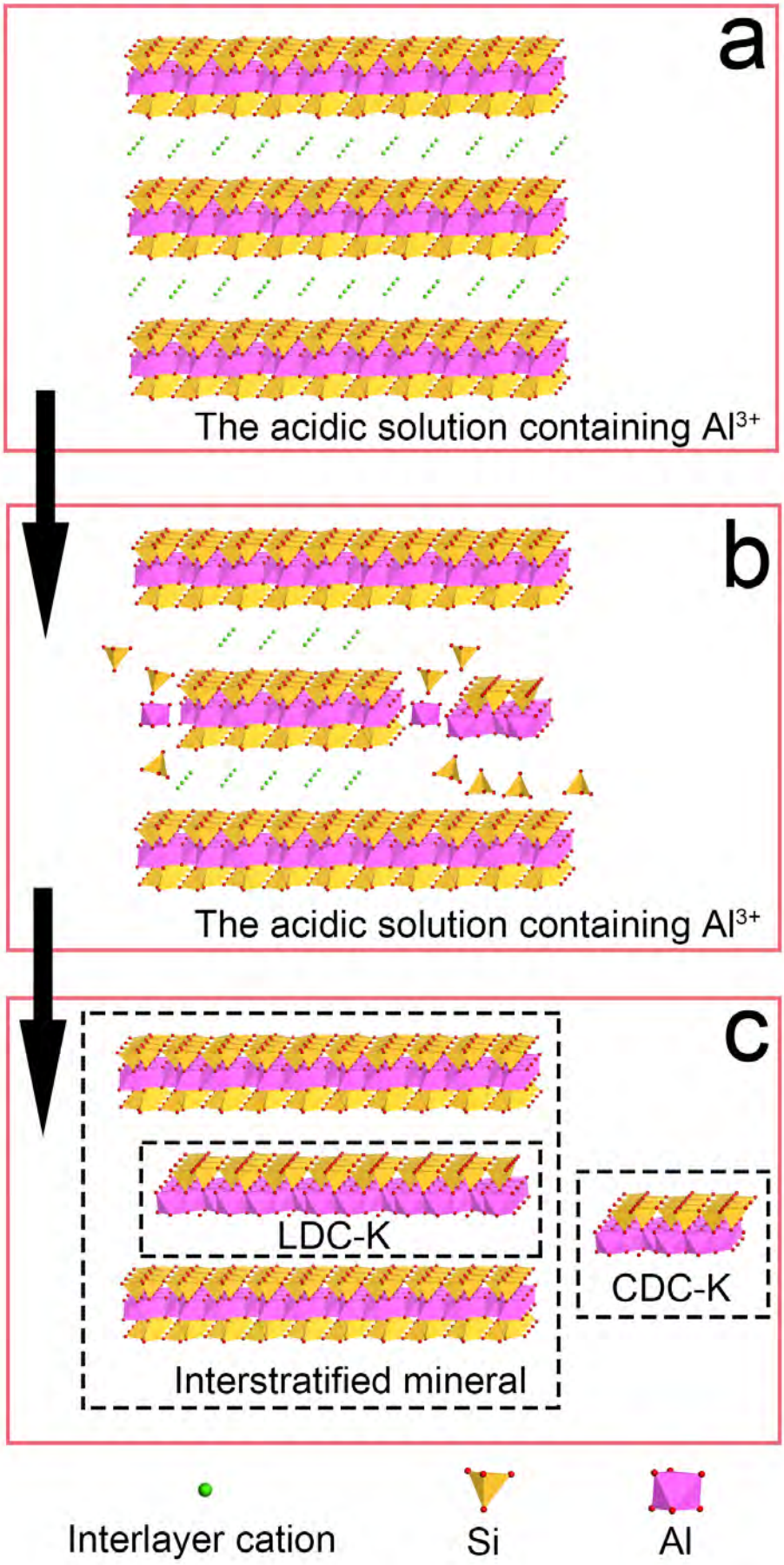

Always consult and cite the final, published document. See http:/www.minsocam.org or GeoscienceWorld

This is a preprint, the final version is subject to change, of the American Mineralogist (MSA)
Cite as Authors (Year) Title. American Mineralogist, in press.
DOI: https://doi.org/10.2138/am-2020-7339

1 **TABLE 1.** Chemical compositions of starting materials.

	Al_2O_3	CaO	Fe_2O_3	K_2O	MgO	Na_2O	P_2O_5	SiO_2	TiO_2	H_2O	Total(%)
Mnt	15.98	2.94	4.86	0.21	4.98	3.21	0.03	59.40	0.32	7.88	99.81
Ill	36.60	0.22	0.25	9.57	0.24	0.25	0.20	47.12	0.41	4.83	99.70
Rec	34.49	5.25	0.43	0.79	0.33	1.40	2.26	41.75	4.23	8.28	99.21

2

Always consult and cite the final, published document. See http:/www.minsocam.org or GeoscienceWorld

This is a preprint, the final version is subject to change, of the American Mineralogist (MSA)
Cite as Authors (Year) Title. American Mineralogist, in press.
DOI: https://doi.org/10.2138/am-2020-7339

TABLE 2. Mass losses of dehydrations and dehydroxylations of sample Mnt and its hydrothermal products obtained from acidic solutions containing Al^{3+} after different durations and those of sample Al-Mnt.

Samples	Dehydration (wt%) (30-300°C)	Dehydroxylation (wt%) (300-800°C)	Mnt/%[a]	Kao/%[b]
Mnt	10.46	6.32	100.00	0.00
Mnt-Al-1d	17.52	4.78	89.34	9.14
Mnt-Al-2d	13.85	6.41	64.46	33.39
Mnt-Al-4d	8.41	8.87	27.48	69.78
Mnt-Al-8d	4.51	11.05	0.00	100.00
Al-Mnt	19.15	4.22	100.00	0.00

[a] Relative content of montmorillonite layers in clay minerals in each sample; [b] Relative content of kaolinite layers. Here, it is assumed relative contents of montmorillonite and kaolinite layers in clay minerals are 100.00 % in Al-Mnt and Mnt-Al-8d, respectively, based on XRD patterns in Fig 1. Relative contents of montmorillonite and kaolinite layers in other hydrothermal products were calculated from mass losses of hydrations and dehydrations of sample Al-Mnt (not Mnt) and Mnt-Al-8d, due to different hydration interlayer states of montmorillonite before (Na-montmorillonite) and after hydrothermal treatment (Al-montmorillonite).

Always consult and cite the final, published document. See http:/www.minsocam.org or GeoscienceWorld